Telomerase activity

Telomerase activity was detected using a TRAPeze telomerase detection kit (Chemicon, Temecula, CA, USA) according to the manufacturer's protocol. The samples were separated using Tris-buffered EDTA-based 8% acrylamide non-denaturing gel electrophoresis. The gels were stained with SYBR Green I (1:10000; TaKaRa, Shiga, Japan).

Lentivirus transduction

For expression of GFP, the self-inactivating lentiviral vector construct pCS-CDF-UbC-GFP-PRE was used, which contains the *EGFP* gene under the control of the human ubiquitin C (UbC) promoter. Lentiviral vectors pseudotyped with the vesicular stomatitis virus G glycoprotein were generated as described previously (Tahara-Hanaoka *et al.*, 2002). Rabbit ES cells were cultured overnight with rESM-containing lentiviruses at a multiplicity of infection (MOI) of 5, 50, or 200 in flat-bottomed 48-well plates, at 37°C in 6% CO_2 in air. The total volume of culture medium per well was less than 110 µl. Fourteen hours after transduction, 100 µl of rESM was added. Two days after transduction, ES cells were harvested by trypsinization and were re-plated into 12-well plates. The medium was changed daily. Five days after transduction, GFP-positive colonies were removed, mechanically dissociated into small clumps, and then cultured in flat-bottomed six-well plates. GFP-positive cells were subsequently propagated under standard ES cell-passaging conditions.

Cell cloning

EGFP-expressing rabbit ES cell colonies were dissociated into single cells using 0.05% trypsin. The dissociated cells were seeded onto an MEF feeder layer ($6 \times 10^3/cm^2$) in flat-bottomed 96-well plates at clonal density (one cell/well). The colony-forming wells were counted 5–7 days later and cloning efficiencies were calculated. These colonies were amplified by passaging to four-well plates. After they had been passaged several times, expanded ES cells were analysed for alkaline phosphatase activity.

Differentiation *in vitro* and *in vivo*

For embryoid body (EB) formation, ES cells were digested with 0.05% trypsin, resuspended in a solution containing 78% DMEM/F-12, 20% fetal bovine serum (FBS), 2 mmol/l GlutaMax, 1% non-essential amino acids, and 0.1 mmol/l β-mercaptoethanol, and cultured in hanging drops. EB were collected after 4–7 days in suspension culture and transferred to plastic dishes coated with gelatin to promote adherence. Culture was continued for an additional 7–14 days in order to promote differentiation. The outgrowths were then fixed and stained using haematoxylin and eosin.

To induce differentiation of ES cells into specific cell lineages, these cells were cultured in several differentiation media. The culture medium for neural differentiation was DMEM/F-12 containing 0.5% FBS, 2 mmol/l GlutaMax, 1% non-essential amino acids, 0.1 mmol/l β-mercaptoethanol, and 10 ng/ml human platelet-derived growth factor-BB (R and D Systems, Minneapolis, USA). The culture medium for epithelial differentiation was DMEM/F-12 containing 10% FBS, 2 mmol/l GlutaMax, 1% non-essential amino acids, 0.1 mmol/l β-mercaptoethanol, and 10^3 IU/ml ESGRO. Fourteen days after induction, differentiated cells were fixed in paraformaldehyde and stained with the following antibodies: mouse anti-β-tubulin III (Sigma) for neurons, mouse anti-glial fibrillary acidic protein (GFAP, Santa Cruz) for astrocytes, and rat anti-collagen IV (Novotec, Saint Martin La Garenne, France) and anti-human mucin (MUC1, Abcom, Cambridge, UK) for epithelial cells. For visualization of cells, F-actin was stained using phalloidine.

For teratoma formation, $2–5 \times 10^6$ ES cells (rES8–2 and rES9–2) were injected under the kidney capsule of 5- to 8-week-old severe combined immunodeficient (SCID) mice. After 10–12 weeks, teratomas were dissected and fixed in paraformaldehyde. Paraffin sections were stained with haematoxylin and eosin (H & E).

RNA extraction and quantitative PCR

Total RNA was isolated from rabbit ES cells cultured in the presence of KSR or FBS, using ISOGEN (Nippon Gene, Toyama, Japan). First-strand cDNA was synthesized using a Takara RNA PCR kit (Takara, Shiga, Japan) with an oligo(dT)-3 site adaptor primer. Synthesized cDNA was subjected to quantitative PCR. The ABI Prism 7900HT was used to determine the mRNA expression levels using the QuantiTect SYBR Green PCR Kit (Qiagen, Hilden, Germany), and a cycling programme of 94°C for 10 min, 40 cycles of 94°C for 30 s, 58°C for 30 s, and 72°C for 30 s. The forward and reverse primers used were as follows: rabbit *Oct4*: TTCCCAACGAGAGGATTTTG and GAACTTCACCTTCCCCACCAA; rabbit *G3*pdh: GGAGCCAAACGGGTCATCATCTC and GAGGGGCCATCCACAGTCTTCT. Data were normalized relative to *G3*pdh amplification.

Production of chimeric embryos

In order to attempt the production of chimeric rabbits, GFP-expressing lines (rES8–2, rES9–2, and rES9–7) of ES cells were trypsinized to dissociate them as single cells or small clumps of cells. Recipient embryos were recovered from superovulated (see above) females at the eight-cell or blastocyst stage following natural mating. Five to 20 ES cells were injected into the cavities of the blastocysts or into the perivitelline spaces of the eight-cell embryos using a piezo-driven micromanipulator. Blastocysts shortly after injection, or blastocysts derived from injected eight-cell embryos were transferred into the uteri of day 3 pseudopregnant females that had been treated with 100 IU HCG and finger stimulation 3 days before transplantation. The chimerism of the newborn pups was determined by the presence of GFP fluorescence.

Animal experiments

All animals were maintained and used for experiments in accordance with the guidelines for animal experimentation of the RIKEN Bioresource Centre.

Results

The fate of ES cells was determined by feeder cell density. Zona-free blastocysts were readily obtained by applying pressure in the perivitelline space. The blastocysts thus collected were normal in appearance and the trophectoderm was completely free of zona components (**Figure 1A**). Three to 6 days later, outgrowth of ICM cells was observed on the culture plate (**Figure 1B**). In an initial series of experiments, these emerging ES-like cells were passaged onto feeder cells (36×10^3 cell/cm^2), as is the routine practice for mouse ES cells. The ES cell-like colonies all disappeared within four or five passages. However, it was observed that ES cell-like colonies reappeared over the feeder-free areas on the culture plates from which colonies had been removed. Therefore, it was assumed that a high concentration of feeder cells represses ES cell growth.

To assess the correlation between ES-like cell growth and feeder cell concentration, ES cells were seeded onto varying concentrations of feeder cells (0, 3, 6, 12, or 36×10^3/cm^2). As expected, when ES cells were seeded onto a high concentration of feeder cells (36×10^3/cm^2), ES cell colonies disappeared within several passages. On the other hand, ES cells cultured under feeder-free conditions spread sparsely on the bottom as flattened cells and did not form any colonies (**Figure 2A**). The ES cell colonies formed most efficiently when they were cultured at a feeder cell density of 6×10^3/cm^2. This density also improved colony morphology (densely packed cells of homogenous sizes), alkaline phosphatase activity, and cell proliferation (**Figure 2A,B**). Therefore, this feeder cell density was used for the next series of experiments. Eleven ES cell lines were established from 91 blastocysts (**Table 1**). Rabbit ES cells grew as monolayer colonies with a doubling time of 13–15 h (**Figure 2C**). ES cell lines that were passaged 20 times or more were used for detailed characterizations (**Table 2**). A rabbit ES cell line, rES 8–2, was cultured for more than 200 days (up to the 56th passage) using a conventional trypsin digestion protocol and was then cryopreserved (**Table 1**). The majority of cells (>70%) from this line showed a normal karyotype during early passages (around passage 7), and even at passage 55, about 60% of cells maintained the normal karyotype. Five ES cell lines were examined for pluripotency and proliferative ability and it was found that these qualities were maintained after freezing and thawing (data not shown). As expected from their proliferation potentials, the ES cells exhibited high levels of telomerase activity at all passages (**Figure 2D**).

Expression of marker proteins

Expression of ES-cell marker proteins was examined using antibodies against SSEA-1, SSEA-3, SSEA-4, OCT4, and NANOG. Rabbit ES cells were weakly positive for SSEA1 and SSEA4, strongly positive for NANOG and OCT4, and negative for SSEA3 (**Figure 3**). The cells were negative or very weakly positive for Tra-1–60 and Tra-1–81 (data not shown). These marker proteins were associated with the pluripotency of cultured cells: a high fluorescent intensity of anti-OCT4 was observed in closely packed colonies, whereas no fluorescence was detected in sparsely diffused ES cells (**Figure 3**).

Gene transduction and clonal expansion

To examine whether the rabbit ES cells could be genetically modified using exogenous genes, gene transduction experiments were performed using a lentiviral vector. Five

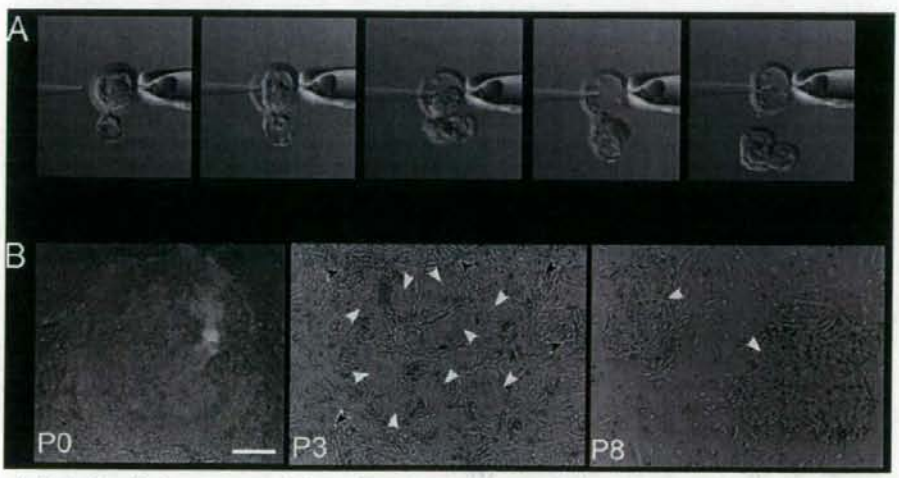

Figure 1. Derivation of primary outgrowth from rabbit blastocyst. (**A**) Artificial zona-shedding of a blastocyst using a Piezo micromanipulator. The blastocyst was smoothly flushed through a slit by introducing medium into the perivitelline space from the opposite side. (**B**) The appearance of cell colonies at different stages, from the outgrowth of ICM cells to the emergence of stable ES colonies. P0: primary rabbit ES cell colony grown on feeder cells 7 days after plating. P3: mixed populations of stem-cell-like (black arrowheads) and differentiating (white arrowheads) colonies at passage 3. P8: only stem-cell-like colonies remained after the eighth passage (black arrowhead). Scale bar: 50 μm.

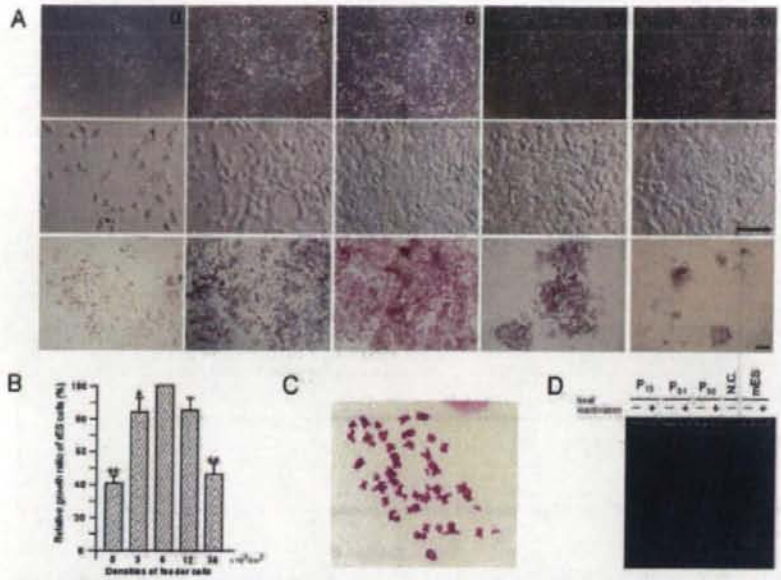

Figure 2. Effects of feeder cell density on rabbit ES cell colonies. (**A**) Feeder cell density is critical for colony formation from ES cells. Rabbit ES cells were seeded onto various concentrations of feeder cells (0, 3, 6, 12, or $36 \times 10^3/cm^2$) and examined under a phase-contrast microscope (lower magnification, upper panel) or Hoffman optics (higher magnification, middle panel), and for alkaline phosphatase activity (lower panel). Large colonies of densely packed cells that had the highest alkaline phosphatase activity were formed when ES cells were seeded onto a concentration of feeder cells of $6 \times 10^3/cm^2$. Under other feeder cell conditions, ES cells differentiated but did not form colonies (0 and $3 \times 10^3/cm^2$), or formed small colonies ($12 \times 10^3/cm^2$ and $36 \times 10^3/cm^2$). Scale bars: 200 μm, 100 μm, and 200 μm respectively. Representative images of rES9–7 at passage 13. (**B**) Relative growth ratios of rabbit ES cells exposed to different densities of feeder cells. The highest proliferation ratio was observed when ES cells were seeded onto $6 \times 10^3/cm^2$ feeder cells (= 100%). Asterisks indicate significant differences ($^*P < 0.05$ and $^{**}P < 0.01$) compared with the $6 \times 10^3/cm^2$ group. Cell numbers were counted at the time of passage (passaged more than five times) and the average growth ratios were calculated for each group. (**C**) The normal number ($2n = 44$) of metaphase chromosomes in a rabbit ES cell from rES8–2 at passage 20. (**D**) Detection of the telomerase activity of rabbit ES cells using the telomeric-repeat amplification (TRAP) protocol. The cells had high telomerase activity at all passages. Heat-inactivated (+) samples were used as negative controls. N.C., lysis buffer only; mES, mouse ES cells used as a positive control.

Figure 3. Detection of pluripotency markers in rabbit ES cells. Cells were positive for NANOG, SSEA-1, SSEA-4, and OCT4 but not for SSEA-3. In the panel on the right, OCT4-positive undifferentiated cells are exclusively localized within the compacted colony (arrows), whereas OCT4-negative differentiating cells are sparsely distributed (arrowheads). From the top: anti-OCT4 staining, Hoechst dye staining, and Hoffman optics image. Representative images of rES8–2 cells at passage 8. Scale bar: 100 μm

Table 1. Results of rabbit embryonic stem (ES) cell line derivation

Series	*No. blastocysts used*	*No. (%) outgrowth*	*No. (%) ES cell lines*	*Line*	*No. passages*[a]	*Days of culture*[a]
rES8	22	7 (31.8)	4 (18.2)	rES8-1	6	33
				rES8-2	60	227
				rES8-3	6	33
				rES8-4	6	33
rES9	30	8 (27.6)	4 (13.3)	rES9-1	30	113
				rES9-2	32	120
				rES9-6	20	70
				rES9-7	20	70
rES10	39	10 (25.6)	3 (7.7)	rES10-1	12	44
				rES10-2	12	44
				rES10-3	12	44
Total	91	25 (27.4)	11 (12.1)	–	–	–

[a]Before freezing for cryopreservation.

Table 2. Characterization of rabbit embryonic stem cell lines that had been passaged 20 times or more.

Cell line	*AP activity*	*Immuno-staining*	*EB formation*	*In-vitro differentiation*	*Tera-toma*	*Karyo-type*	*RT-PCR*	*Telom-erase (Oct4)*	*Cloning*	*Gene modification*
rES8-2	+	+	+	+	+	+	+	+	+	+
rES9-1	+	+	+	+	+	+	+	nd	+	+
rES9-2	+	nd	+	nd	nd	+	+	nd	nd	+
rES9-6	+	nd	nd	nd	nd	+	nd	nd	nd	+
rES9-7	+	nd	+	nd	nd	+	+	nd	nd	+

AP = alkaline phosphatase; EB = embryoid body; + = detected; nd = not determined.

ES cell lines were infected with a lentiviral vector containing the EGFP gene and were cultured for 2 days. Although many GFP-positive colonies formed in all lines at an MOI of 200, very few cells were transfected at an MOI of 50. No GFP-positive cells were observed at an MOI of 5 (data not shown). The GFP gene was successfully integrated into the genome of all cell lines, as indicated by consistent expression of GFP fluorescence over many passages.

The cloning efficiency of rabbit ES cells was also examined using GFP-positive cells. Single cells from the rES8–2 (passage 12) and rES9–1 (passage 9) lines were seeded onto 96-well plates at clonal density and their growth was recorded daily using a fluorescence microscope (**Figure 4**). More than one-fifth (21.2 ± 2.3%) of the individual cells formed colonies within 5–10 days and could be passaged successfully. These cells exhibited alkaline phosphatase activity and were indistinguishable from their parental cell lines in morphology.

Differentiation *in vitro* and *in vivo*

Rabbit ES cells readily started to differentiate when FBS (instead of KSR) was added to the culture medium, as indicated by the reduction in *Oct4* expression and alkaline phosphatase activity (**Figure 5B,C**). They further differentiated into EB in suspension culture (**Figure 5D**). Plating of EB onto a gelatin-coated culture dish resulted in outgrowths of cells of various types, including multiple cystic structures (**Figure 5E**). These heterologous cell populations included cobblestone-like cells, neuron-like cells, lipid-bearing cells, and eosinophilic granule-producing cells (**Figure 5F–I**). It was also examined whether ES cells could be induced to differentiate into specific cell lineages. In a neural differentiation medium, ES cells differentiated into β-tubulin III-positive neurons and GFAP-positive astrocytes (**Figure 5J**). In the epithelial differentiation medium, they differentiated into MUC1-postive or collagen IV-positive epithelial cells (**Figure 5K–L**).

To examine the differentiation potency of rabbit ES cells *in vivo*, two ES cell lines (rES8–2 and rES9–2) were transplanted into SCID mice. At 10–12 weeks after transplantation, both lines formed teratomas consisting of tissues derived from three germ layers: hair follicles (ectoderm), skeletal muscle fibres (mesoderm), and glands (endoderm) (**Figure 6A–D**).

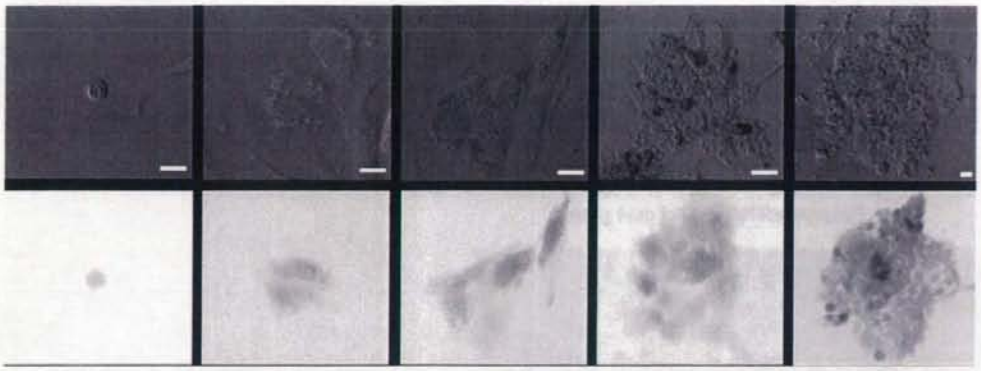

Figure 4. Clonal expansion of rabbit ES cells. Time course of colony formation from a single rabbit ES cell that was transfected with the *EGFP* gene by a lentiviral vector (rES8–2 cells at passage 12). The ES cell was seeded onto feeder cells and cell proliferation was scored at 2, 12, 24, 48, and 120 h. Scale bar: 20 µm.

Development of chimeric embryos

The ability of rabbit ES cells to contribute to fetal development was tested by the production of chimeric embryos. After the transfer of 47 embryos into recipient females, 17 pups were born in four different experiments using three ES cell lines (rES8–2, rES9–2, and rES9–7). However, examination of GFP fluorescence revealed that the ES cells made no contribution to any of their tissues.

Discussion

Human ES cells are potentially useful for regenerative medicine, developmental biology, tissue regeneration, disease pathology, and drug discovery (Thomson *et al.*, 1998). However, the use of human ES cell lines is limited because the destruction of developing human embryos is required for their establishment (Lerou *et al.*, 2008). Recently, induced pluripotent cells (iPS cells) have been generated from human somatic cells, which is expected to overcome the ethical problems associated with cell lines derived from embryos (Takahashi *et al.*, 2007; Park *et al.*, 2008). However, the safety and reliability of their use for tissue regeneration in humans is still to be determined (Stojković and Phinney, 2008). Many attempts have been made to use animal models to overcome limitations associated with human ES cells (Familari and Selwood, 2006). However, stable animal ES cell lines have only been generated from mice and monkeys (Thomson *et al.*, 1995). The use of monkey cell lines may hinder progress because of the limitations of transplantation trials. Mouse ES cells are easily generated from blastocysts and used in regenerative experimental models. However, extrapolation of results obtained using mice to humans is limited because of fundamental differences in colony morphologies, growth requirements, and biochemical characteristics between murine and human ES cells (Koestenbauer *et al.*, 2006).

It has been proposed that rabbit ES cells represent an alternative small animal model for human ES cells, and several reports on their derivation have been published since the first attempt by Cole *et al.* in 1964. However, so far as is known, no stable rabbit ES cell lines have been developed. This is probably because of their limited propagation potential during conventional culture. Although a recent report indicated that rabbit ES cells may be passaged for more than a year (Fang *et al.*, 2006; Wang *et al.*, 2007), it has been difficult to maintain good cell lines for long periods (Jianglin Fan, personal communication). The present report describes an easy and reproducible technique for the establishment of rabbit ES cell lines with indefinite proliferative ability. Derivation of this ES cell line was achieved primarily by optimization of feeder cell conditions and secondarily by an improved zona-shedding method for blastocysts.

Feeder cell layers are extensively used for derivation and maintenance of ES cells or ES-like cells in many species. Feeder cells, mostly of murine or homologous origin, are thought to support ES cells by supplying nutrients and growth factors in a paracrine fashion and by providing scaffolds for ES cell colonization (Choo *et al.*, 2006; Stacey *et al.*, 2006). It was found that high densities of feeder cell layers repressed proliferation of rabbit ES cells, and that rabbit ES cells spread onto areas that were free of feeder cells during culture. This suggests that the feeder cells inhibit proliferation of rabbit ES cells by competing for surface area, or through a contact-mediated mechanism. Nevertheless, feeder cells are apparently indispensable for the maintenance of the pluripotency of rabbit ES cells, as they transformed into fibroblast-like cells in the absence of feeder cells. Thus, feeder cell density was found to be critical for derivation and culture of rabbit ES cells. The optimal window was narrower than expected; density was optimal at 1/6 of confluency and inferior at 1/12 and 1/3 of confluency. Identification of the feeder cell factors necessary for ES cell pluripotency is warranted so that a feeder-free culture system can be established for rabbit ES cells.

Another important finding was that damage to blastocysts must be minimized for successful outgrowth culture. Rabbit blastocysts are surrounded by a strong zona pellucida and a very thick outer mucin coat. *In vivo*, hatching blastocysts escape from these two protein layers through a hole made by trophoblastic

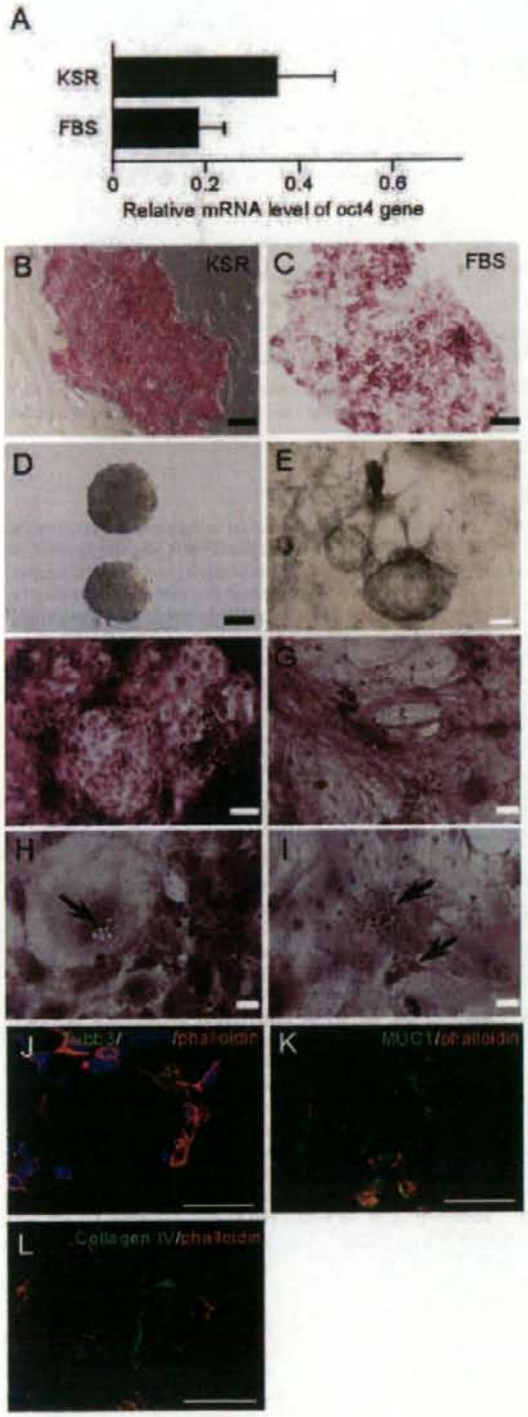

Figure 5. In-vitro differentiation of rabbit ES cells. (**A**) Relative expression levels of rabbit *Oct4* in the presence of KSR or FBS. Reduced expression was observed when rabbit ES cells were cultured in the presence of serum. (**B**, **C**) Alkaline phosphatase activity of rabbit ES cell colonies cultured in the presence of KSR or FBS. The reduced and uneven distribution of alkaline-phosphatase-positive cells is noted in the FBS group. (**D**) Typical EB in hanging drop culture. (**E**) EB forming cystic structures on a tissue culture dish. (**F–I**) H & E staining of EB-derived outgrowths. The cells are cobblestone-like cells (**F**), neuron-like cells (**G**), lipid-bearing cells (arrow in **H**), and eosinophilic granule-containing cells (arrow in **I**). (**J–L**) Direct differentiation *in vitro* of ES cells in differentiation media. Markers specific for neurons (β-tubulin; Tubb3), astrocytes (GFAP), and epithelial cells (Muc1 and collagen IV) are evident. Scale bars: 200 μm in (**E**) and (**J**); 100 μm in (**B**), (**C**), (**D**), (**F**), (**K**) and (**L**); and 20 μm in (**G–I**).

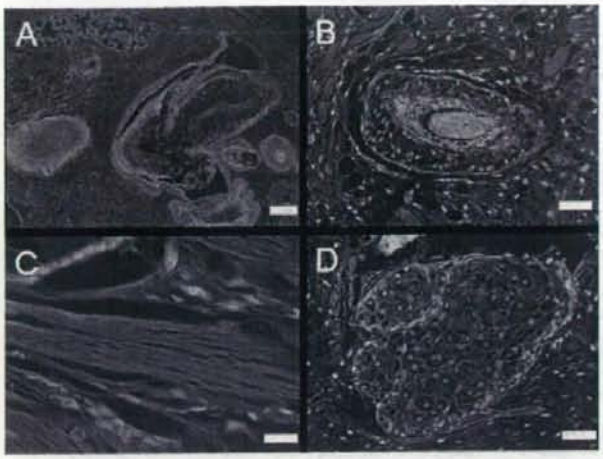

Figure 6. In-vivo differentiation of rabbit ES cells. (**A**) Histology of a teratoma at low magnification. A variety of cell types are evident in the section. (**B–D**) Teratomas at high magnification. A hair follicle (**B**), muscle fibres (**C**), and a gland (**D**) are evident. Scale bars: 200 µm in (**A**); 50 µm in (**B**) and (**D**); and 20 µm in (**C**).

knobs (Steer, 1970). Therefore, exogenous mechanical or enzymatic treatment of these layers may damage blastocysts. In preliminary experiments, the mucin coat and zona pellucida of rabbit blastocysts flushed from the uteri of naturally mated does on day 3.5 post-coitus were removed either chemically using acidic Tyrode's solution (pH 2.4) or enzymatically using pronase (0.5% in PBS). However, because of damage to the blastocysts, it was not possible to establish ES cell lines (unpublished). In this study, embryos were collected before mucin was deposited and a method was used that mimicked natural blastocyst hatching. By applying positive pressure inside the zona, blastocysts easily escaped from the zona through a hole. The blastocysts were healthy in appearance, attached to the bottom of the culture vessel, and formed ICM colonies.

In addition to their usefulness as a regeneration therapy model, ES cells have great potential for the production of genetically modified animals, especially gene-targeted animals. However, the mouse is the only animal species in which germline-contributing chimeras have been produced using ES cells. Attempts have been made to generate chimeric rabbits by ES cell aggregation or injection, but there is no evidence of germline contribution of ES cells (Schoonjans *et al.*, 1996). Recently, murine pluripotent cell lines that have several characteristics in common with human ES cells have been generated from epiblast cells (Brons *et al.*, 2007; Tesar *et al.*, 2007). One of the most intriguing findings was that very few chimeras were obtained from them and germline transmission was not observed. These studies suggest that human ES cells are eventually equivalent to the early post-implantation epiblasts, rather than to their ICM progenitors (Rossant, 2008). If this is also true of rabbit ES cells, it may be difficult to generate germline chimeras in rabbits. Indeed, it has been found that bFGF, the growth factor known to promote human ES cell self-renewal, was also essential for the maintenance of rabbit ES cells (unpublished), whereas the effect of LIF remains unclear. An alternative strategy involves the application of nuclear transfer technology. Fortunately, ES cells are easier to clone using nuclear transfer than other differentiated somatic cells (mouse, bovine) (Saito *et al.*, 2003; Wakayama 2007). As nuclear transfer cloning has been successful in rabbits, knockout rabbits could be produced by combining nuclear transfer and ES cell gene targeting.

The advantages of the ES cell derivation technique are its ease and high reproducibility. Rabbit ES cells with indefinite self-renewing potential can be generated consistently from about 10% of embryos (**Table 1**). This has been confirmed by others (T Kishigami, personal communication). Consequently, rabbit ES cells should be added to the list of stable ES cells in mammalian species. Rabbit ES cells are suitable for use in small animal models to study human cell-transplantation therapy and human diseases and might be combined with gene-targeting techniques in the future.

Acknowledgements

The authors would like to thank Drs Jianglin Fan and Satoshi Kishigami for valuable discussions of this study. This work was supported by a Grant-in-Aid for Scientific Research on Priority Areas (MEXT) and CREST of JST (Japan Science and Technology Agency).

References

Bösze Z, Hiripi L, Carnwath JW *et al.* 2003 The transgenic rabbit as model for human diseases and as a source of biologically active recombinant proteins. *Transgenic Research* **12**, 541–553.

Brons IG, Smithers LE, Trotter MW *et al.* 2007 Derivation of pluripotent epiblast stem cells from mammalian embryos. *Nature* **448**, 191–195.

Carney EW, Foote RH 1991 Improved development of rabbit one-cell embryos to the hatching blastocyst stage by culture in a defined, protein-free culture medium. *Journal of Reproduction and Fertility* **91**, 113–123.

Chang MC 1959 Fertilization of rabbit ova in vitro. *Nature* **184**, 466–467.

Chesné P, Adenot PG, Viglietta C *et al.* 2002 Cloned rabbits produced by nuclear transfer from adult somatic cells. *Nature Biotechnology* **20**, 366–369.

Choo A, Padmanabhan J, Chin A *et al.* 2006 Immortalized feeders for the scale-up of human embryonic stem cells in feeder and feeder-free conditions. *Journal of Biotechnology* **122**, 130–141.

Cole RJ, Edwards RG, Paul J 1966 Cytodifferentiation and embryogenesis in cell colonies and tissue cultures derived from ova and blastocysts of the rabbit. *Developmental Biology* **13**, 385–407.

Cole RJ, Edwards RG, Paul J 1964 Cytodifferentiation in cell colonies and cell strains derived from cleaving ova and blastocysts of the rabbit. *Experimental Cell Research* **37**, 501–504.

Downing GJ, Battey JF Jr 2004 Technical assessment of the first 20 years of research using mouse embryonic stem cell lines. *Stem Cells* **22**, 1168–1180.

Familari M, Selwood L 2006 The potential for derivation of embryonic stem cells in vertebrates. *Molecular Reproduction and Development* **73**, 123–131.

Fang ZF, Gai H, Huang YZ *et al.* 2006 Rabbit embryonic stem cell lines derived from fertilized, parthenogenetic or somatic cell nuclear transfer embryos. *Experimental Cell Research* **312**, 3669–3682.

Graves KH, Moreadith RW 1993 Derivation and characterization of putative pluripotential embryonic stem cells from preimplantation rabbit embryos. *Molecular Reproduction and Development* **36**, 424–433.

Hosoi Y, Miyake M, Utsumi K *et al.* 1998 Development of rabbit oocytes after microinjection of spermatozoa. *Proceedings of the 11th International Congress of Animal Reproduction* **3**, 331–333.

Inoue K, Ogonuki N, Yamamoto Y *et al.* 2002 Improved postimplantation development of rabbit nuclear transfer embryos by activation with inositol 1,4,5-trisphosphate. *Cloning and Stem Cells* **4**, 311–317.

Kasai M, Hamaguchi Y, Zhu SE *et al.* 1992 High survival of rabbit morulae after vitrification in an ethylene glycol-based solution by a simple method. *Biology of Reproduction* **46**, 1042–1046.

Koestenbauer S, Zech NH, Juch H *et al.* 2006 Embryonic stem cells: similarities and differences between human and murine embryonic stem cells. *American Journal of Reproductive Immunology* **55**, 169–180.

Lerou PH, Yabuuchi A, Huo H *et al.* 2008 Human embryonic stem cell derivation from poor-quality embryos. *Nature Biotechnology* **26**, 212–214.

Liu JL, Kusakabe H, Chang CC *et al.* 2004 Freeze-dried sperm fertilization leads to full-term development in rabbits. *Biology of Reproduction* **70**, 1776–1781.

Ogonuki N, Inoue K, Miki H *et al.* 2005 Differential development of rabbit embryos following microinsemination with sperm and spermatids. *Molecular Reproduction and Development* **72**, 411–417.

Park IH, Zhao R, West JA *et al.* 2008 Reprogramming of human somatic cells to pluripotency with defined factors. *Nature* **451**, 141–146.

Rossant J 2008 Stem cells and early lineage development. *Cell* **132**, 527–531.

Rudert M 2002 Histological evaluation of osteochondral defects: consideration of animal models with emphasis on the rabbit, experimental setup, follow-up and applied methods. *Cells Tissues Organs* **171**, 229–240.

Saito S, Sawai K, Ugai H *et al.* 2003 Generation of cloned calves and transgenic chimeric embryos from bovine embryonic stem-like cells. *Biochemical and Biophysical Research Communications* **309**, 104–113.

Schoonjans L, Albright GM, Li JL *et al.* 1996 Pluripotential rabbit embryonic stem (ES) cells are capable of forming overt coat color chimeras following injection into blastocysts. *Molecular Reproduction and Development* **45**, 439–443.

Shiomi M, Ito T, Yamada S *et al.* 2004 Correlation of vulnerable coronary plaques to sudden cardiac events. Lessons from a myocardial infarction-prone animal model (the WHHLMI rabbit). *Journal of Atherosclerosis and Thrombosis* **11**, 184–189.

Shufaro Y, Reubinoff BE 2004 Therapeutic applications of embryonic stem cells. *Best Practice and Research Clinical Obstetrics and Gynaecology* **18**, 909–927.

Stacey GN, Cobo F, Nieto A *et al.* 2006 The development of 'feeder' cells for the preparation of clinical grade hES cell lines: challenges and solutions. *Journal of Biotechnology* **125**, 583–588.

Steer HW 1970 The trophoblastic knobs of the preimplanted rabbit blastocyst: a light and electron microscopic study. *Journal of Anatomy* **107**, 315–325.

Stojković M, Phinney DG 2008 Reprogramming battle: egg vs. virus. *Stem Cells* **26**, 1–2.

Tahara-Hanaoka S, Sudo K, Ema H *et al.* 2002 Lentiviral vector-mediated transduction of murine CD34– hematopoietic stem cells. *Experimental Hematology* **30**, 11–17.

Takahashi K, Tanabe K, Ohnuki M *et al.* 2007 Induction of pluripotent stem cells from adult human fibroblasts by defined factors. *Cell* **131**, 861–872.

Tesar PJ, Chenoweth JG, Brook FA *et al.* 2007 New cell lines from mouse epiblast share defining features with human embryonic stem cells. *Nature* **448**, 196–199.

Thomson JA, Itskovitz-Eldor J, Shapiro SS *et al.* 1998 Embryonic stem cell lines derived from human blastocysts. *Science* **282**, 1145–1147.

Thomson JA, Kalishman J, Golos TG *et al.* 1995 Isolation of a primate embryonic stem cell line. *Proceedings of the National Academy of Sciences of the USA* **92**, 7844–7848.

Vackova I, Ungrova A, Lopes F 2007 Putative embryonic stem cell lines from pig embryos. *Journal of Reproduction and Development* **53**, 1137–1149.

Wakayama T 2007 Production of cloned mice and ES cells from adult somatic cells by nuclear transfer: how to improve cloning efficiency? *Journal of Reproduction and Development* **53**, 13–26.

Wang B, Zhou J 2003 Specific genetic modifications of domestic animals by gene targeting and animal cloning. *Reproductive Biology and Endocrinology* **1**, 103.

Wang S, Tang X, Niu Y *et al.* 2007 Generation and characterization of rabbit embryonic stem cells. *Stem Cells* **25**, 481–489.

Weekers F, Van Herck E, Coopmans W *et al.* 2002 A novel in vivo rabbit model of hypercatabolic critical illness reveals a biphasic neuroendocrine stress response. *Endocrinology* **143**, 764–774.

Yamagata K, Nakanishi T, Ikawa M *et al.* 2002 Sperm from the calmegin-deficient mouse have normal abilities for binding and fusion to the egg plasma membrane. *Developmental Biology* **250**, 348–357.

Yang F, Hao R, Kessler B *et al.* 2007 Rabbit somatic cell cloning: effects of donor cell type, histone acetylation status and chimeric embryo complementation. *Reproduction* **133**, 219–230.

Declaration: The authors report no financial or commercial conflicts of interest.

Received 28 March 2008; refereed 14 May 2008; accepted 19 August 2008.

Available online at www.sciencedirect.com
ScienceDirect
PLACENTA
Placenta 29 (2008) 753–759

Ultrastructure of Placental Hyperplasia in Mice: Comparison of Placental Phenotypes with Three Different Etiologies

N. Wakisaka [a], K. Inoue [a,b], N. Ogonuki [a], H. Miki [a], Y. Sekita [c], K. Hanaki [d], A. Akatsuka [e], T. Kaneko-Ishino [f], F. Ishino [c], A. Ogura [a,b,d,*]

[a] *Bioresouce Center, RIKEN, Tsukuba, Ibaraki 305-0074, Japan*
[b] *Graduate School of Life and Environmental Science, University of Tsukuba, Tsukuba, Ibaraki, 305-8572, Japan*
[c] *Medical Research Institute, Tokyo Medical and Dental University, Chiyoda-ku, Tokyo 101-0062, Japan*
[d] *The Center for Disease Biology and Integrative Medicine, Faculty of Medicine, University of Tokyo, Bunkyo-ku, Tokyo, Japan*
[e] *School of Medicine, Tokai University, Isehara, Kanagawa 259-1193, Japan*
[f] *School of Health Sciences, Tokai University, Isehara, Kanagawa 259-1193, Japan*

Accepted 22 May 2008

Abstract

Hyperplastic placentas have been reported in several experimental mouse models, including animals produced by somatic cell nuclear transfer, by inter(sub)species hybridization, and by somatic cytoplasm introduction to oocytes followed by intracytoplasmic sperm injection. Of great interest are the gross and histological features common to these placental phenotypes – despite their quite different etiologies – such as the enlargement of the spongiotrophoblast layers. To find morphological clues to the pathways leading to these similar placental phenotypes, we analyzed the ultrastructure of the three different types of hyperplastic placenta. Most cells affected were of trophoblast origin and their subcellular ultrastructural lesions were common to the three groups, e.g., a heavy accumulation of cytoplasmic vacuoles in the trophoblastic cells composing the labyrinthine wall and an increased volume of spongiotrophoblastic cells with extraordinarily dilatated rough endoplasmic reticulum. Although the numbers of trophoblastic glycogen cells were greatly increased, they maintained their normal ultrastructural morphology, including a heavy glycogen deposition throughout the cytoplasm. The fetal endothelium and small vessels were nearly intact. Our ultrastructural study suggests that these three types of placental hyperplasias, with different etiologies, may have common pathological pathways, which probably exclusively affect the development of certain cell types of the trophoblastic lineage during mouse placentation.

Keywords: Somatic cell nuclear transfer; Placentomegaly; Electron microscopy; Mouse; ICSI

1. Introduction

Since the birth of the first lamb cloned from somatic cells, the technique of somatic cell nuclear transfer (SCNT) has been applied successfully to a wide range of mammalian species [1]. However, the efficiency of producing cloned offspring remains extremely low because of the frequent loss of embryos at the pre- and postimplantation stages. The cloning-associated abnormalities most commonly observed across species are placental defects [2]. Cloned cattle placentas, in particular, have been examined in detail from the macroscopic to the electron-microscopic levels and vascular anomalies are considered the major primary defects associated with SCNT placentas [3–5]. Placental dysfunction may affect the viability of cloned embryos at any stage during gestation. Even at term, morphologically normal cloned offspring often shows a variety of placental abnormalities. One of the typical placental phenotypes associated with cloned animals is hyperplasia, which inevitably occurs in mice cloned from somatic cells [6] or early

* Corresponding author. Bioresouce Center, RIKEN, Tsukuba, Ibaraki 305-0074, Japan. Tel.: +81 29 836 9165.
E-mail address: ogura@rtc.riken.go.jp (A. Ogura).

0143-4004/$ - see front matter © 2008 Elsevier Ltd. All rights reserved.
doi:10.1016/j.placenta.2008.05.008

primordial germ cells [7]. Interestingly, a very similar phenotype has also been reported in the placentas of mice produced by intersubspecies hybridization [8,9], those carrying an *Esx1* gene mutation [10] and those derived from intracytoplasmic sperm injection (ICSI) following injection of somatic cell cytoplasm into an oocyte (cytoplasm injection ICSI; ciICSI) [11]. These findings suggest that we might understand the mechanisms of placental hyperplasia by identifying the genes commonly dysregulated in these three models of hyperplasia. However, despite intensive efforts, only a few downstream genes have been identified and the upstream mechanisms of hyperplasia remain to be clarified [12,13].

Until now, the morphological information available about placental hyperplasia in mice has accumulated based on observations at the light microscopic level. However, because the placenta is a structurally complex organ composed of many cell types of different origins, detailed information on the ultrastructure of each placental region is necessary for precise classification of abnormal placentation. This study was undertaken to characterize the ultrastructural features of the hyperplastic placentas associated with SCNT, intersubspecies ICSI and ciICSI. Common ultrastructural features, if any, would imply the presence of certain common mechanisms underlying the abnormal phenotypes induced by different experimental models.

2. Materials and methods

All animal experiments were performed in accordance with the guidelines of the RIKEN Bioresource Center, Japan. Mice were maintained under specific-pathogen-free conditions, provided with water and commercial laboratory mouse chow ad libitum and housed under controlled lighting conditions (daily light period of 07:00–21:00 h).

2.1. SCNT

B6D2F1 female mice, 8–12 weeks of age, were used for the collection of recipient oocytes and donor cumulus cells. The mice were superovulated by an injection of 7.5 IU of equine chorionic gonadotropin, followed by 7.5 IU of human chorionic gonadotropin (hCG) approximately 48 h later. Oocytes were collected from the oviducts approximately 15 h after the hCG injection and were released from the cumulus cells by treatment with 0.1% bovine testicular hyaluronidase in KSOM medium [14]. The enucleation of the oocytes, nuclear transfer into the enucleated oocytes and oocyte activation were carried out according to the methods reported previously [15,16].

2.2. Intersubspecies ICSI and ciICSI

Mature oocytes were collected for the ICSI experiments from the oviducts of B6D2F1 female mice, as described above. Epididymal spermatozoa from HMI (*Mus musculus castaneus*) males at 60–90 days of age were cryopreserved and thawed on the day of the experiment [17]. They were retrieved into NIM medium [18,19] and injected into the oocytes, as reported previously [20]. In another series of experiments, ciICSI was performed, as described previously [11]. Cytoplasm masses from one or two cumulus cells were injected into an oocyte 1–2 h before conventional ICSI using B6D2F1 spermatozoa.

2.3. In vitro fertilization (IVF)

Embryos were generated by conventional IVF and used for controls. Mature oocytes were obtained from B6D2F1 females as described above and inseminated with C57BL/6 spermatozoa as described previously [17].

2.4. Embryo culture and transfer

Oocytes that survived the experiments were cultured in KSOM at 37 °C under 5% CO_2 in air until embryo transfer. Embryos that had reached the two-cell stage by 24 h (ICSI and ciICSI) or the four-cell stage by 48 h (SCNT) were transferred into the oviducts of day 0.5 pseudopregnant ICR females. On day 19.5, the placentas were collected from the recipient females for histological and electron microscopy examinations.

2.5. Light microscopic examination and in situ hybridization

The placentas, at least five from each group, were fixed with 4% paraformaldehyde in 0.1 M phosphate buffer (pH 7.4), dehydrated and embedded in paraffin. Sections of 4 μm thickness were cut and stained with hematoxylin and eosin (H&E). Sections of 8 μm thickness were processed for in situ hybridization using an antisense digoxigenin-labeled *Tpbpa* riboprobe, as described previously [20]. Sections from placentas fixed with Rossman's fixative [21] were stained for PAS reaction using a commercially available staining kit (Muto Pure Chemicals, Tokyo, Japan).

2.6. Electron microscopy examination

The placentas, at least two from each group, were processed for electron microscopy. They were trimmed into small square blocks with sides of about 2 × 2 × 1 mm, washed with phosphate-buffered saline (PBS) and fixed in 2.5% glutaraldehyde in 0.05 M phosphate buffer (pH 7.4) overnight at 4 °C. The blocks were postfixed in 1% osmium tetroxide for 2 h at 4 °C, dehydrated through ethanol and acetone and embedded in Quetol 812 (Nisshin EM, Tokyo, Japan). Semi-thin (1 μm) sections were cut, stained with toluidine blue and examined using light microscopy for the purpose of tissue selection from the entire transverse areas of the placenta except for the peripheral extremes. At least three blocks were selected from each placenta sample for electron microscopy. Ultrathin sections were cut, stained with uranyl acetate and lead citrate and observed with a JEM-1200 EX transmission electron microscope (JEOL, Tokyo, Japan).

3. Results

The mouse placenta consists of three fetal compartments: the labyrinthine layer, the spongiotrophoblast (ST) layer and the giant cell layer. In situ hybridization for *Tpbpa*, a specific marker gene for the ST layer, clearly visualized the boundary between the ST and labyrinthine layers (Fig. 1). Mouse hyperplastic placentas in each experimental group retained this basic compartmentalization pattern, but showed common major pathological changes, which were obvious even at the light microscopic level. First, the boundary between the two fetal layers was irregularly interdigitated, in sharp contrast to the very smooth boundary of in vitro-fertilized placentas. Second, the ST layer was greatly enlarged, primarily because of increased numbers of glycogen cells. These were identified as large vacuolated cells on conventional H&E sections as glycogen disappears during conventional tissue processing (Fig. 1A), or as PAS-reacted cells on glycogen-preserved sections (Fig. 1B). The enlargement of the ST layer was more prominent in the SCNT group than in the other two groups (Fig. 1A).

We used electron microscopy to obtain more detailed information on the pathology of these three types of placental hyperplasia. The interhemal membrane of the labyrinthine layer in the mouse placenta is composed of three trophoblastic layers (I, II and III) and the fetal endothelium, forming the

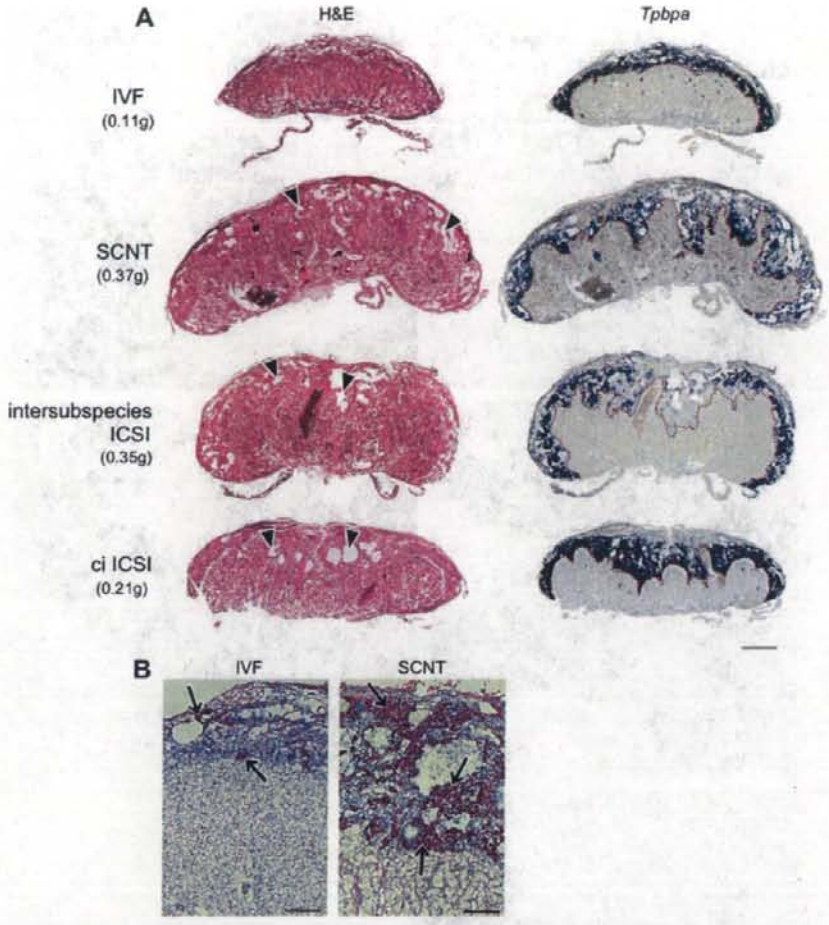

Fig. 1. (A) Histology of term placentas from IVF, SCNT, intersubspecies ICSI and ciICSI experiments. H&E staining (left column) and in situ hybridization detection of *Tpbpa*, a marker for the ST layer (right column). The red dotted lines indicate the boundary between the labyrinthine and ST layers. The three experimental models of hyperplasia share common abnormalities: enlargement of the ST layer, large clusters of glycogen cells (arrowheads), and an irregular boundary between the labyrinthine and ST layers. An arrow in the intersubspecies ICSI placenta indicates the maternal blood space that normally exists in mouse placentas. (B) PAS-reacted sections from IVF and SCNT experiments, showing glycogen cells in the ST layer (arrows). The number of glycogen cells greatly increased in the SCNT placentas. Bars = 1 mm (A) and 200 μm (B).

so-called hemotrichorial membrane (Fig. 2A). Trophoblast layer I is a cytotrophoblast layer lining the maternal blood spaces. Trophoblast layers II and III are syncytiotrophoblast layers situated between layer I and the fetal endothelium. The hyperplastic placentas in all groups maintained the hemotrichorial structure. However, the three trophoblast layers all accumulated many cytoplasmic vacuoles, with layer I being most severely affected (Fig. 2B–D). The trophoblastic layers had sometimes lost many of their intercellular desmosomes. This caused the detachment of the two layers, especially layers II and III in the intersubspecies ICSI group (Fig. 2C and F). Placentas of the SCNT group tended to maintain the normal close contact between these trophoblastic layers (Fig. 2B and E). The fetal epithelial cells were relatively normal and maintained a continuous basement membrane (Fig. 2B–D).

The ST layer of all the experimental groups was characterized by the formation of large clusters of glycogen cells. This feature was more pronounced in the SCNT group than in the other two groups, confirming the findings of light microscopy. However, the individual glycogen cells showed no obvious pathological changes at the ultrastructural level and had typical appropriately localized glycogen deposits in their cytoplasm (Fig. 3). In contrast, the spongiotrophoblast cells, another major cell type of the ST layer, displayed a variety of ultrastructural changes. These generalized features included remarkable dilatation of the rough endoplasmic reticulum

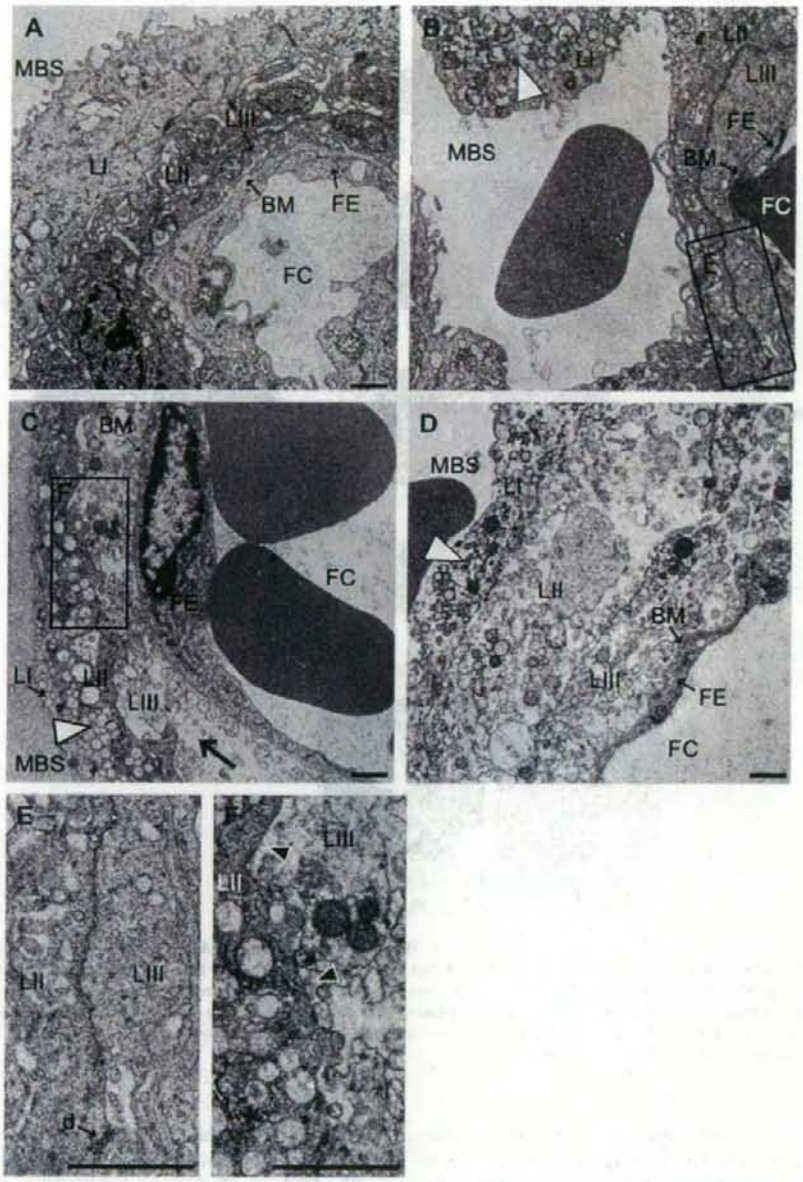

Fig. 2. Electron-microscopic observations of the labyrinthine layer of term placentas from IVF (A), SCNT (B), intersubspecies ICSI (C) and ciICSI (D). In the three models of hyperplastic placentas, multiple vacuolar structures in trophoblastic layer I are noted (arrowheads in B–D). E is a higher magnification of the rectangle area of B, showing normal association of layers II and III with a desmosome (d). F is a higher magnification of the rectangle area of C, showing the boundary of layers II and III. Junctional complexes have been lost and there are spaces between the two layers (arrowheads). BM, basement membrane; FC, fetal capillary; FE, fetal endothelium; LI, LII and LIII, trophoblast layers I, II and III, respectively; MBS, maternal blood space. Bars = 1 μm.

(ER) cisternae, which contained homogenous electron-opaque material (Fig. 4B–E) and increased numbers of Golgi apparatuses around the nucleus (Fig. 4F). As a result, they were increased two- to threefold in diameter and this was most pronounced in the SCNT group (Fig. 4B). However, within the scope of our investigation, very few cells were undergoing degenerative changes in the ST layer.

We also examined the ultrastructure of the fetal umbilical vessels penetrating the labyrinthine and ST layers, but no differences were observed among the groups (data not shown).

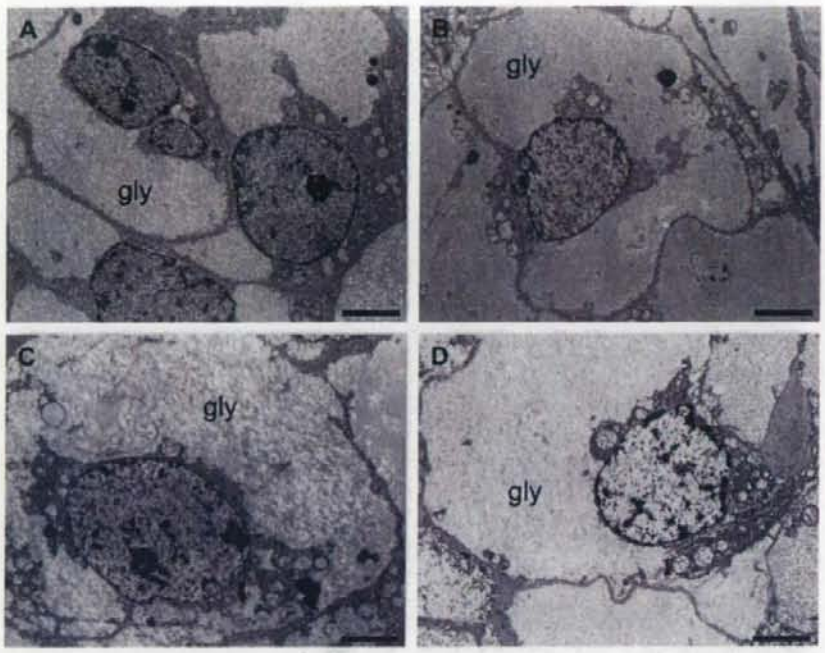

Fig. 3. Glycogen cells in the ST layer from IVF (A), SCNT (B), intersubspecies ICSI (C) and ciICSI (D). A large mass of glycogen (gly) fills nearly the entire area of the cytoplasm except for a small perinuclear area. Glycogen cells from four groups are indistinguishable with each other by their size and morphology. Bars = 5 μm.

4. Discussion

Over the past decade, mouse placental hyperplasia of different etiologies has been an interesting model for the study of developmental biology, pathology and genetics. The ultrastructure of the hyperplastic placentas revealed several important features common to the three experimental groups we observed. First, the affected cell types in the labyrinthine layer were the trophoblastic cells rather than the endothelial cells. The affected trophoblastic cells in layers I, II and III showed excessive accumulation of intracytoplasmic vacuoles. Such vacuoles are normally formed in mouse placentas as they develop to late gestation [22], but their numbers were much greater in the hyperplastic placentas. Li and Behringer [10] found the same vacuolar lesions in hyperplastic placentas lacking *Esx1*, a homeobox gene expressed in the chorionic trophoblast. They assumed that this alteration might be a consequence of defects in intracellular transport. Because significant repression of *Esx1* is also reported in SCNT placentas [23], this gene may be responsible in general for the pathological changes in the trophoblastic layers in hyperplastic placentas.

Another ultrastructural feature common to all three groups was spongiotrophoblast cell hypertrophy, associated with extraordinary expansion of rough ER. Because spongiotrophoblast cells near term are characterized by expanded rough ER [22], it is likely that this cellular activity is abnormally upregulated in hyperplastic placentas, or there are some abnormalities in protein processing or exocytosis. Spongiotrophoblast cells produce many proteins with endocrine activity, e.g., prolactin-like hormones, lactogens and cytokines [24]. The glycogen cells, the numbers of which are greatly elevated in hyperplastic placentas, had a normal morphology and therefore probably functioned as energy sources for the placenta [22].

It should be noted that the endothelial cells in the labyrinthine capillaries and the fetal vessels penetrating the two layers showed no obvious pathological changes. Therefore, components of allantoic origin were not significantly affected in the hyperplastic placentas we examined. Thus, certain cell types of the trophoblastic lineage cells were exclusively affected in these hyperplastic placentas. We have reported that term placentas of both Sertoli cell- and cumulus cell-derived clones show a significant reduction in mRNA levels of three imprinted genes (*Peg1/Mest*, *Meg1/Grb10* and *Meg3/Gtl2*) and four nonimprinted genes (*Igfbp2*, *Igfbp6*, *Vegfr2/Flk1* and *Esx1*) [23]. These genes are expressed preferentially in the trophoblastic cells and are the determinants of placental size or function. It is possible that at least some of them are responsible for the pathological changes observed in this study, although they might represent downstream genes involved in placental hyperplasia. Recently, *Car2* and *Ncam1* were also identified as genes associated with the placental hyperplasia caused by interspecies hybridization and SCNT [13].

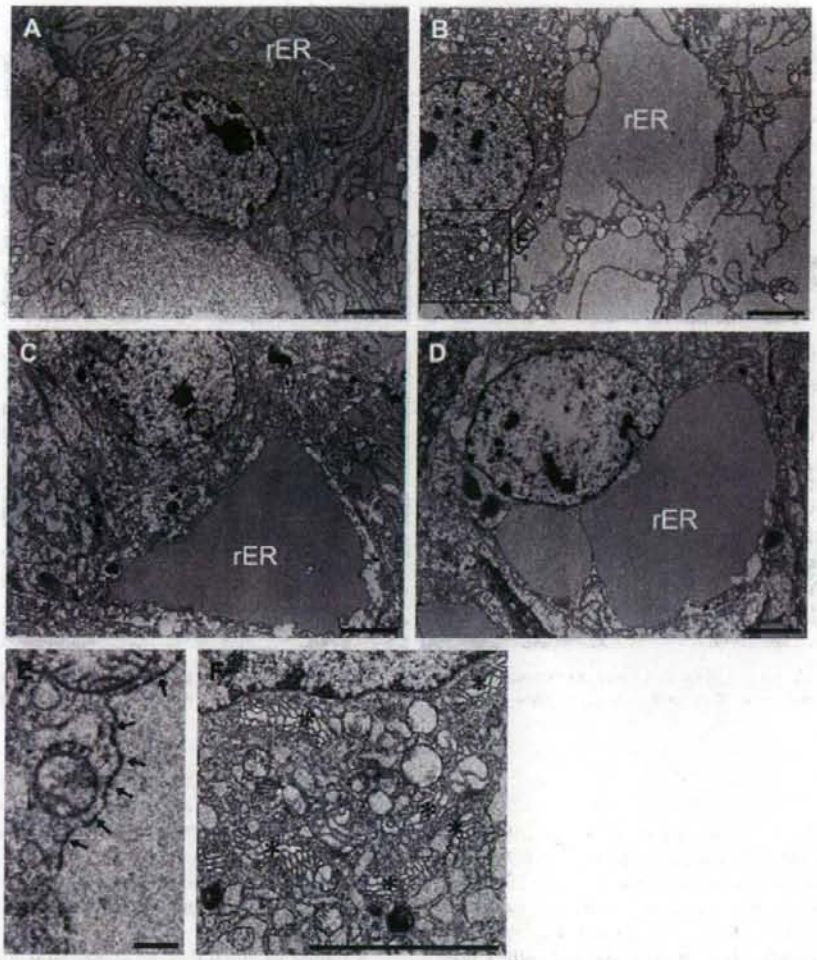

Fig. 4. Spongiotrophoblast cells in the ST layer from IVF (A), SCNT (B), intersubspecies ICSI (C) and ciICSI (D). Those in hyperplastic placentas commonly show remarkable dilatation of the rough endoplasmic reticulum (rER) cisternae, which contained homogenous electron-opaque material (B–D). The size of spongiotrophoblastic cells is increased two- to threefold in diameter and this was most pronounced in the SCNT group. (E) A higher magnification of the smaller rectangle in B, showing presence of ribosome particles on the rER membrane (arrows). (F) A higher magnification of the larger rectangle in B, showing increased numbers of Golgi apparatuses around the nucleus (asterisks). Bars = 5 μm (A–D, F) and 10 μm (E).

Therefore, the next subject to be studied is the primary mechanisms underlying these placental hyperplasias with different etiologies. Our ultrastructural observations indicate that they may exclusively affect trophoblastic lineage cells during mouse placentation. Interestingly, placental hyperplasia in SCNT and XO mice is preceded by the poor development of the ectoplacental cone, the earliest trophoblastic tissue formed [20,25]. We also observed this in the early placentation of intersubspecies hybrids (unpublished). Thus, it is likely that early hypoplastic placentation and subsequent hyperplastic placentation constitute a series of trophoblastic abnormalities, which may be attributable to unknown upstream mechanisms. In SCNT, placental abnormalities are often attributed to "reprogramming errors" in the donor genome. However, the treatment of reconstructed embryos with a histone deacetylase inhibitor, which greatly improves the cloning efficiency in mice, never alleviates this placental phenotype [26]. As mentioned above, only a small amount of somatic cytoplasm in an embryo can cause placental hyperplasia. These results suggest that placental hyperplasia is not an "erroneous" phenotype but an inevitably "induced" consequence of the experiments. According to Ono and Kono [27], mouse embryos cloned from inner-cell-mass cells developed hyperplastic placentas, but those from four-cell or eight-cell blastomeres did not. Epigenetic analyses of the preimplantation embryos or early trophoblastic tissues generated in several different experiments,

which differentially affect placentation, might provide us with important clues to understanding this unique placental abnormality.

Acknowledgments

The wild-derived HMI strains used in this study were provided by RIKEN Bioresource Center, with the support of the National BioResources Project of the MEXT, Japan. This work was supported by a Grant-in-Aid for Scientific Research on Priority Areas (MEXT).

References

[1] Meissner A, Jaenisch R. Mammalian nuclear transfer. Dev Dyn 2006; 235:2460–9.
[2] Yang X, Smith SL, Tian XC, Lewin HA, Renard JP, Wakayama T. Nuclear reprogramming of cloned embryos and its implications for therapeutic cloning. Nat Genet 2007;39:295–302.
[3] Hill JR, Burghardt RC, Jones K, Long CR, Looney CR, Shin T, et al. Evidence for placental abnormality as the major cause of mortality in first-trimester somatic cell cloned bovine fetuses. Biol Reprod 2000;63: 1787–94.
[4] Miglino MA, Pereira FT, Visintin JA, Garcia JM, Meirelles FV, Rumpf R, et al. Placentation in cloned cattle: structure and microvascular architecture. Theriogenology 2007;68:604–17.
[5] Arnold DR, Fortier AL, Lefebvre R, Miglino MA, Pfarrer C, Smith SL. Placental insufficiencies in cloned animals – a workshop report. Placenta 2008;29(Suppl.):S108–10.
[6] Tanaka S, Oda M, Toyoshima Y, Wakayama T, Tanaka M, Yoshida N, et al. Placentomegaly in cloned mouse concepti caused by expansion of the spongiotrophoblast layer. Biol Reprod 2001;65:1813–21.
[7] Miki H, Inoue K, Kohda T, Honda A, Ogonuki N, Yuzuriha M, et al. Birth of mice produced by germ cell nuclear transfer. Genesis 2005;41:81–6.
[8] Zechner U, Reule M, Orth A, Bonhomme F, Strack B, Guenet J-L, et al. An X-chromosome linked locus contributes to abnormal placental development in mouse interspecific hybrid. Nat Genet 1996;12:398–403.
[9] Shinmen A, Honda A, Ohkawa M, Hirose M, Ogonuki N, Yuzuriha M, et al. Efficient production of intersubspecific hybrid mice and embryonic stem cells by intracytoplasmic sperm injection. Mol Reprod Dev 2007; 74:1081–8.
[10] Li Y, Behringer RR. *Esx1* is an X-chromosome-imprinted regulator of placental development and fetal growth. Nat Genet 1998;20:309–11.
[11] Van Thuan N, Wakayama S, Kishigami S, Ohta H, Hikichi T, Mizutani E, et al. Injection of somatic cell cytoplasm into oocytes before intracytoplasmic sperm injection impairs full-term development and increases placental weight in mice. Biol Reprod 2006;74:865–73.
[12] Singh U, Fohn LE, Wakayama T, Ohgane J, Steinhoff C, Lipkowitz B, et al. Different molecular mechanisms underlie placental overgrowth phenotypes caused by interspecies hybridization, cloning and *Esx1* mutation. Dev Dyn 2004;230:149–64.
[13] Singh U, Sun T, Shi W, Schulz R, Nuber UA, Varanou A, et al. Expression and functional analysis of genes deregulated in mouse placental overgrowth models: *Car2* and *Ncam1*. Dev Dyn 2005;234:1034–45.
[14] Lawitts JA, Biggers JD. Culture of preimplantation embryos. Methods Enzymol 1993;225:153–64.
[15] Wakayama T, Perry ACF, Zuccotti M, Johnson KR, Yanagimachi R. Full-term development of mice from enucleated oocytes injected with cumulus cell nuclei. Nature 1998;394:369–74.
[16] Inoue K, Ogonuki N, Mochida K, Yamamoto Y, Takano K, Kohda T, et al. Effects of donor cell type and genotype on the efficiency of mouse somatic cell cloning. Biol Reprod 2003;69:1394–400.
[17] Mochida K, Ohkawa M, Inoue K, Valdez Jr DM, Kasai M, Ogura A. Birth of mice after in vitro fertilization using C57BL/6 sperm transported within epididymides at refrigerated temperatures. Theriogenology 2005; 64:135–43.
[18] Kuretake S, Kimura Y, Hoshi K, Yanagimachi R. Fertilization and development of mouse oocytes injected with isolated sperm heads. Biol Reprod 1996;55:789–95.
[19] Ogonuki N, Mochida K, Miki H, Inoue K, Fray M, Iwaki T, et al. Spermatozoa and spermatids retrieved from frozen reproductive organs or frozen whole bodies of male mice can produce normal offspring. Proc Natl Acad Sci U S A 2006;103:13098–103.
[20] Wakisaka-Saito N, Kohda T, Inoue K, Ogonuki N, Miki H, Hikichi T, et al. Chorioallantoic placenta defects in cloned mice. Biochem Biophys Res Commun 2006;349:106–14.
[21] Hess A. The ground substance of the central nervous system revealed by histochemical staining. J Comp Neurol 1953;98:69–91.
[22] Coan PM, Ferguson-Smith AC, Burton GJ. Ultrastructural changes in the interhemal membrane and junctional zone of the murine chorioallantoic placenta across gestation. J Anat 2005;207:783–96.
[23] Inoue K, Kohda T, Lee J, Ogonuki N, Mochida K, Noguchi Y, et al. Faithful expression of imprinted genes in cloned mice. Science 2002; 295:297.
[24] Soares MJ. The prolactin and growth hormone families: pregnancy-specific hormones/cytokines at the maternal–fetal interface. Reprod Biol Endocrinol 2004;2:51.
[25] Jamieson RV, Tan SS, Tam PP. Retarded postimplantation development of X0 mouse embryos: impact of the parental origin of the monosomic X chromosome. Dev Biol 1998;201:13–25.
[26] Kishigami S, Mizutani E, Ohta H, Hikichi T, Thuan NV, Wakayama S, et al. Significant improvement of mouse cloning technique by treatment with trichostatin A after somatic nuclear transfer. Biochem Biophys Res Commun 2006;340:183–9.
[27] Ono Y, Kono T. Irreversible barrier to the reprogramming of donor cells in cloning with mouse embryos and embryonic stem cells. Biol Reprod 2006;75:210–6.

STEM CELLS AND DEVELOPMENT 17:367-381(2008)

DOI: 10.1089/scd.2007.0119

Original Research Report

Sustained Macroscopic Engraftment of Cynomolgus Embryonic Stem Cells In Xenogeneic Large Animals after In Utero Transplantation

YUJIRO TANAKA,[1,7] SHINICHIRO NAKAMURA,[2] HIROAKI SHIBATA,[1,3] YUKIKO KISHI,[1] TAMAKO IKEDA,[1] SHIGEO MASUDA,[1] KYOKO SASAKI,[1] TOMOYUKI ABE,[4] SATOSHI HAYASHI,[5] YOSHIHIRO KITANO,[6] YOSHIKAZU NAGAO,[4] and YUTAKA HANAZONO[1]

ABSTRACT

Because embryonic stem (ES) cells are able to proliferate indefinitely and differentiate into any type of cell, they have the potential for providing an inexhaustible supply of transplantable cells or tissues. However, methods for the in vitro differentiation of human ES cells are still quite limited. One possible strategy would be to generate differentiated cells in vivo. In view of future clinical application, we investigated the possibility of using xenogeneic large animals for this purpose. We transplanted nonhuman primate cynomolgus ES cells into fetal sheep at 43–67 gestational days (full term 147 days, $n = 15$). After birth, cynomolgus tissues, which were mature teratomas, had been engrafted in sheep when more than 1×10^6 ES cells were transplanted at <50 gestational days. Despite the sustained engraftment, both cellular and humoral immune responses against the ES cells were detected, and additional transplantation was not successful in the animals. At 2 weeks post-transplantation, the ES cell progeny proliferated when transplanted at 48 (<50) gestational days, whereas they were cleared away when transplanted at 60 (>50) gestational days. These results support the rapid development of the xenogeneic immunological barrier in fetal sheep after 50 gestational days. Notably, a large number of Foxp3$^+$ regulatory T cells were present around the ES cell progeny, but macrophages were absent when the transplant was conducted at <50 gestational days, implying that regulatory T cells and premature innate immunity might have contributed to the sustained engraftment. In conclusion, long-term macroscopic engraftment of primate ES cells in sheep is feasible despite the xenogeneic immunological barrier.

[1]Division of Regenerative Medicine, Center for Molecular Medicine, Jichi Medical University, Tochigi 329-0498, Japan.
[2]Corporation for Production and Research of Laboratory Primates, Ibaraki 305-0843, Japan.
[3]Tsukuba Primate Research Center, National Institute of Biomedical Innovation, Ibaraki 305-0843, Japan.
[4]Department of Agriculture, Utsunomiya University, Tochigi 321-4415, Japan.
[5]Department of Obstetrics and Gynecology, and [6]Department of Surgery, National Center for Child Health and Development, Tokyo 157-8535, Japan.
[7]Department of Pediatric Surgery, Graduate School of Medicine, University of Tokyo, Tokyo 113-8655, Japan.
The contents of this study were in part presented at the 5th annual meeting of the International Society for Stem Cell Research (ISSCR).

INTRODUCTION

A MAJOR BARRIER TO MOST TISSUE OR CELLULAR transplantation therapies is the shortage of donors. Because embryonic stem (ES) cells are able to proliferate indefinitely and differentiate into any type of cell [1,2], they have potential for providing an inexhaustible supply of transplantable cells or tissues. However, methods for the in vitro differentiation of human (h) ES cells are still quite limited. One possible strategy would be to generate differentiated cells in vivo in animals. In fact, rodent and nonhuman primate allogeneic transplantation models have demonstrated that transplanted ES cells respond to local cues in vivo and showed site-specific differentiation [3,4]. Therefore, the local microenvironment or niche would be important and potentially useful for directed differentiation of ES cells. Given that transplantation experiments using hES cells should be conducted in a xenogeneic setting, there are two major obstacles to this strategy: (1) the xenogeneic immunological barrier [5,6] and (2) the mismatch of microenvironment between the donor and recipient [7].

Although large animals would be clinically relevant as recipients of hES cells for a large supply of therapeutic cells or tissues, there have been very few reports of hES cell-derived engraftment in adult large animals [8]. Generally, such engraftment can be barely achieved by treatment with immunosuppressants. On the other hand, in animal fetuses, it has been considered that the immune system is so premature as not to induce an immune response at the early stages of pregnancy [9,10]. In fact, the in utero transplantation of human hematopoietic stem cells (HSCs) into sheep fetuses before 65 days of gestation (full term, 147 days) led to the generation of human/sheep hematopoietic chimeras (up to 20%). This result also suggests that the fetal sheep microenvironment could provide a proper niche at least for human hematopoietic differentiation [11,12]. Although such chimerism was documented in other animals such as primates, pigs, and mice, the levels of engraftment in sheep were much higher than those in other animals [13,14]. Recently, we and others have shown that cultured primate ES cells also engrafted after in utero transplantation to sheep fetuses, generating microscopic primate/sheep chimeras [15,16]. Furthermore, it has been reported that mouse ES cells engrafted in ischemic hearts of sheep [17] but not in those of baboons [18]. Thus, sheep may be good recipient animals in which stem cells can engraft. In addition, in the fetal period, in vivo microenvironments such as the cytokine milieus are optimized for rapid growth and development of fetuses [19] and this might be favorable for the growth and differentiation of transplanted stem cells. However, primate ES cell-derived macroscopic tissue formation in discordant large animals or systematic studies regarding engraftment and immune responses after in utero transplantation of primate ES cells have not been reported.

In this study, we have transplanted nonhuman primate (cynomolgus macaque) ES cells into fetal sheep and examined whether primate cells can engraft and develop tissues in sheep. In this setting, we have also examined what kind of immune response, if any, is triggered by transplanted primate ES cells.

MATERIALS AND METHODS

Animals

Pregnant Suffolk ewes were purchased from Japan Lamb (Hiroshima, Japan). Fetal sheep at 43–67 days of gestation (full term, 147 days) were used as transplantation recipients. All experiments in this study were performed in accordance with the Jichi Medical University Guide for Laboratory Animals. Experimental procedures were approved by the Animal Care and Use Committee of Jichi Medical University.

Cells

A cynomolgus ES cell (cyES cell) line CMK6 and its subline CMK6G stably expressing green fluorescent protein (GFP) [20] were maintained on a feeder layer of mitomycin C (Kyowa, Tokyo, Japan)-treated mouse (BALB/c, Clea, Tokyo, Japan) embryonic fibroblasts as previously described [21]. Confluent ES cells were dissociated from the feeder layer using 0.1% collagenase type IV (Invitrogen, Carlsbad, CA) for transplantation.

Transplantation and delivery

Before transplantation, ewes were anesthetized with a 0.5–1.0% halothane–oxygen mixture. After a midline laparotomy incision, cells were injected into the fetuses subcutaneously at 1–4 sites/fetus through the uterine wall under ultrasound guidance. The fetuses were delivered at full term or by cesarean section at the indicated days after transplantation.

In situ hybridization and immunohistochemistry

Tissues were fixed with 4% paraformaldehyde and embedded in paraffin. For genomic in situ hybridization, the deparaffinized sections were digested and hybridized with the biotinylated human DNA probe (Dako, Copenhagen, Denmark). The probe was detected with the GenPoint System (Dako) according to the manufacturer's instructions, and nuclei were stained with Hematoxylin. Primary antibodies (Abs) for immunohistochemistry were anti-mouse Oct-3 monoclonal Ab (mAb) (BD Pharmingen, San Diego, CA), rabbit anti-human glial fibrillary acidic protein (GFAP) Ab (Dako), anti-human neuron-specific enolase (NSE) mAb (Dako), anti-human α-smooth muscle actin (α-SMA) mAb (Dako), anti-human desmin mAb (Dako), anti-human vimentin mAb (Dako), rabbit anti-human α-fetoprotein (α-FP) Ab (Dako), and rabbit anti-GFP Ab (Clontech, Palo Alto, CA). The anti-mouse Oct-3 mAb has been confirmed to react to a cynomolgus counterpart [22]. Primary Abs used to

detect sheep immune cells were rabbit anti-human CD3 Ab (Dako), anti-human CD79 mAb (Dako), rabbit anti-human lysozyme Ab (Dako), and rabbit anti-human myeloperoxidase (MPO) Ab (Novocastra Laboratories, Newcastle, UK), all of which have been confirmed to react to sheep counterparts [23]. The primary Abs were detected with the Dako EnVision+ System HRP (Dako) and visualized with 3,3′-diaminobenzide tetrahydrochloride (Dojindo, Kumamoto, Japan). Nuclei were counterstained with Hematoxylin.

Regarding immunofluorescent staining of frozen sections, tissues were fixed with 4% paraformaldehyde. Primary Abs were anti-human leukocyte antigen (HLA)-A, -B, and -C mAbs (BD Pharmingen), which have been confirmed to react to cynomolgus counterparts, anti-ovine CD4 mAb (Serotec, Oxford, UK), anti-ovine CD8 mAb (Serotec), and rat anti-mouse Foxp3 Ab (eBioscience, San Diego, CA). The sections were incubated with Alexa Flour 488- or 555-conjugated secondary Abs (Invitrogen), nuclei-stained with DAPI (Donjindo), and observed with a confocal laser scanning microscope (Nikon, Tokyo, Japan).

Quantitative PCR

Genomic DNA was extracted from samples with the QIAamp DNA mini kit (Qiagen, Hilden, Germany) and subjected to quantitative DNA-PCR for the cynomolgus-specific β2-microglobulin sequence using the QuantiTect SYBR Green PCR kit (Qiagen) and the ABI Prism 7000 (Applied Biosystems, Foster, CA). Cynomolgus DNA was serially diluted with sheep genomic DNA and used to make the standard amplification curves. The primer set was 5′-GTC TGG ATT TCA TCC ATC TG-3′ and 5′-GGT GAA TTC AGT GTA GTA CAA G-3′ and amplification conditions were 40 cycles of 95°C for 60 sec, 60°C for 60 sec, and 72°C for 60 sec.

Flow cytometry

The expression of major histocompatibility complex (MHC) class I and Oct-3 in cultured graft cells and cyES cells was analyzed using a FACS Calibur flow cytometer (BD Pharmingen). For MHC class I, cells were incubated with phycoerythrin (PE)-conjugated anti-HLA-A, -B, and -C mAbs (BD Pharmingen) for 30 min at 4°C. For Oct-3, cells were first fixed using the fixation/permeabilization buffer (eBioscience) for 2 h at 4°C and then incubated with Alexa Fluor 647 (Invitrogen)-conjugated anti-mouse Oct-3 mAb (BD Pharmingen) for 60 min at 4°C. Other cell-surface antigens of fetal sheep peripheral blood leukocytes were also analyzed using the flow cytometer. Fetal sheep peripheral blood (150 μl) were treated with BD Pharm Lyse™ Lysing Buffer (BD Pharmingen) to lyse red blood cells and then incubated with the following conjugated mAbs for 30 min at 4°C: PE-conjugated anti-ovine CD5 mAb (Serotec), Alexa Fluor 647 (Invitrogen)-conjugated anti-ovine CD11b mAb (Serotec), fluorescein isothiocyanate (FITC)-conjugated anti-human CD14 mAb (Serotec), and FITC-conjugated anti-ovine CD45R mAb (Serotec), all of which have been confirmed to react to sheep counterparts. Data acquisition and analysis were performed using CellQuest software (BD Pharmingen). Isotype-matched, fluorescence-conjugated, irrelevant Abs served as negative controls.

Mixed lymphocyte reaction

Mononuclear cells were isolated from heparinized sheep peripheral blood on 55% Percoll (GE Healthcare, Piscataway, NJ) and resuspended in RPMI-1640 medium with 10% fetal bovine serum (FBS). Then, 1×10^5 responder cells and 1×10^5 irradiated (4,000 cGy) stimulator cells were placed in each well of 96-well U-bottomed plates and incubated at 37°C for 5 days. Plates were pulsed with 1 μCi/well of [^{3}H]-thymidine for 24 h and cellular intake of [^{3}H]-thymidine was quantified with a β-scintillation counter (Aloka, Tokyo, Japan). Used as stimulator cells were autologous peripheral blood mononuclear cells (PBMCs), cyES cells, cynomolgus PBMCs, and cultured adherent cells of the grafts that were confirmed to be of cynomolgus origin by karyotyping (SRL, Tokyo, Japan). Cynomolgus PBMCs were isolated on Ficoll-Paque PLUS (GE Healthcare). The mixed lymphocyte reaction (MLR) was assessed with a stimulation index, which was calculated by dividing the mean count per minute of the sample over that of the autologous PBMCs (negative control). Significant differences were examined using the *t*-test.

Xenoantibody detection

Immunoglobulin (Ig) G and IgM xenoantibodies against cyES cells in sheep were determined by flow cytometry. cyES cells (2.5×10^5) were incubated with 10 ml of 1:10 diluted serum taken from the cyES cell-transplanted or naive (control) sheep. In sheep, maternal antibodies do not pass through the placenta, but they do pass through the milk of the mothers [24]. Serum of newborn sheep was taken before they took first milk to exclude the contamination of maternal antibodies. After secondary staining with PE-conjugated donkey anti-ovine IgG Ab (Abcam, Cambridge, UK) and Alexa Fluor 647 (Invitrogen)-conjugated anti-ovine IgM mAb (Serotec), cells were examined with the FACS Calibur flow cytometer. Data acquisition and analysis were performed using the CellQuest software (BD Pharmingen). Nonviable cells were excluded from analysis by propidium iodide (Sigma, St. Louis, MO) co-staining.

Identification of ovine foxp3

On the basis of the cattle *foxp3* sequence in GenBank (accession nos. DQ322170 and XM582445), the primer set 5′-CCA AGT CAC TGG GCC TGC CCT TGA ACA-3′ and 5′-TTC TCT TCT TGG CTC TGA GAT CAG GGG C-3′ was designed for the ovine *foxp3* complete coding sequence (expected amplicon size, 1,353 bp). Total RNA was extracted from sheep PBMCs using the EZ1 RNA universal tissue kit (Qiagen) and reverse-transcribed using the RNA LA PCR kit (Takara, Shiga, Japan) with an oligo(dT) primer. The resulting cDNA was subjected to PCR with this primer set. The PCR product was sequenced with the ABI Prism 310 (Applied Biosystems). Sequence analysis was performed with the Genetyx-Mac software (Genetyx, Tokyo, Japan).

Cross-reactivity of Foxp3 Ab

The cloned ovine *foxp3* cDNA was inserted into the plasmid pCMV-IRES-EGFP and introduced into 293T cells. Trans-

fected cells were fixed using the fixation/permeabilization buffer (eBioscience), stained with PE-conjugated rat anti-mouse Foxp3 Ab (eBioscience), and examined for cross reactivity of the Ab to the ovine Foxp3 using the FACS Calibur flow cytometer.

RESULTS

Macroscopic cynomolgus/sheep chimeras

Pregnancy of ewes could be judged at 35 days of gestation and subcutaneous injection of cells into sheep fetuses was technically feasible under ultrasound guidance at 45 days of gestation in our group. We used cyES cells as a transplantation source. Although there are considerable differences in growth and differentiation conditions between mouse and primate ES cells [25,26], human and cynomolgus ES cells have remarkable similarities [21]. Therefore, studies using cyES cells would be desirable as a predictive model for hES cell behavior. Undifferentiated cyES cells were transplanted subcutaneously into sheep fetuses at 43–67 days of gestation. At birth (3 months post-transplant), palpable tumors were found at some of the transplantation sites (Fig. 1A). The overall incidence of tumor formation was 4/15 sheep (6/36 transplantation sites) (Table 1). Notably, no tumor developed when cyES cells were transplanted after 50 days of gestation (Fig. 1B, left).

To examine whether the tumors were derived from transplanted cyES cells, in situ hybridization with a cynomolgus-specific genomic DNA probe was performed. Because a cynomolgus-specific genomic probe had not been available, we first examined whether a probe developed for humans [27] can specifically detect cynomolgus sequences by testing the monkey and sheep liver tissue sections (Fig. 1C, upper). The monkey liver cell nuclei were positive with the probe, whereas signals were not detected in the sheep liver, thus demonstrating that this human probe can be used to distinguish cynomolgus from sheep cells. As shown in Fig. 1C (lower panel), the tumor cells were clearly positive with the probe, indicating their cynomolgus origin, except for blood cells, most of the feeding vessels, and granulation tissues. To exclude the possibility of their fusion with sheep cells, we examined the karyotype of tumor cells (Fig. 1D). On average, 83% of tumor cells in the engrafted sheep (n = 3) had normal cynomolgus 42 chromosomes, a pattern identical to that of the transplanted cyES cells [21]. On the other hand, cultured sheep cells (n = 3) usually consisted of 54 chromosomes. Taken together, the tumors were cyES cell-derived grafts but were fed by the host sheep vessels. The largest graft was 30 × 28 × 9 cm in size and weighed 3.5 kg (sheep no. 5), which implied favorable local microenvironments of fetal sheep for the growth of cyES cells.

Next, we transplanted different numbers of cyES cells into two or four different sites per fetal sheep (Table 1). As a result, the minimal cell number needed to engraft was found to be 1.4×10^6. Among the cyES cell-engrafted sheep, no engraftment was observed at any sites receiving less than 1×10^6 cells (Fig. 1B, right). Thus, the transplanted cell number was also critical for engraftment. A similar result was reported for the allogeneic transplantation of mouse ES cells [28].

The grafts were excised or biopsied from all the engrafted sheep before 1.5 months of age. The grafts contained all three germ layer cells, composing mature tissue structures such as neural epithelia, cartilage, ductal epithelia, and hepatocyte-like cells (Fig. 2A). Immunohistochemistry revealed that the graft cells were all negative for Oct-3, a pluripotent marker of ES cells [29,30]. On the other hand, they were positive for the differentiation markers ectodermal GFAP, NSE, endodermal α-FP, and mesodermal αSMA, vimentin, and desmin (Fig. 2B). Endodermal cells were found much less frequently than ectodermal and mesodermal cells, which might be a reflection of the subcutaneous transplantation sites [31]. Although transplanted cyES cells were originally negative for MHC class I, many of the cells became positive in the grafts after birth (Fig. 2B).

Histology I: fetal period

The cyES cell-derived grafts in sheep were observed only when the cells were transplanted in utero before 50 days of gestation. It has been believed that early sheep fetuses are immunologically naive and that host immune responses can be circumvented. This concept has received support from the immunological ontogeny in fetal sheep. Morphologically mature lymphocytes first appear in peripheral blood at 32 days of gestation, monocytes at 63 days, and neutrophils at as late as 123 days [32]. IgG and IgM are detected in peripheral blood at 56 and 77 days, respectively, but primary Ab responses remain immature at the onset, and IgG production in response to an antigen challenge occurs only after 87 days [33]. However, a histological examination regarding immune responses after in utero xenogeneic transplantation has not been performed. Here, we transplanted cyES cells expressing GFP (CMK6G, 6×10^6 cells/site) into fetal sheep at either 48 (<50) or 60 (>50) days of gestation, and examined the in vivo fate of transplanted cells and host immune responses at 5 days and 2 weeks after the transplantation.

The transplant sites of delivered fetuses were determined under a fluorescence microscope or by detecting petechiae resulting from the puncture at transplant. When

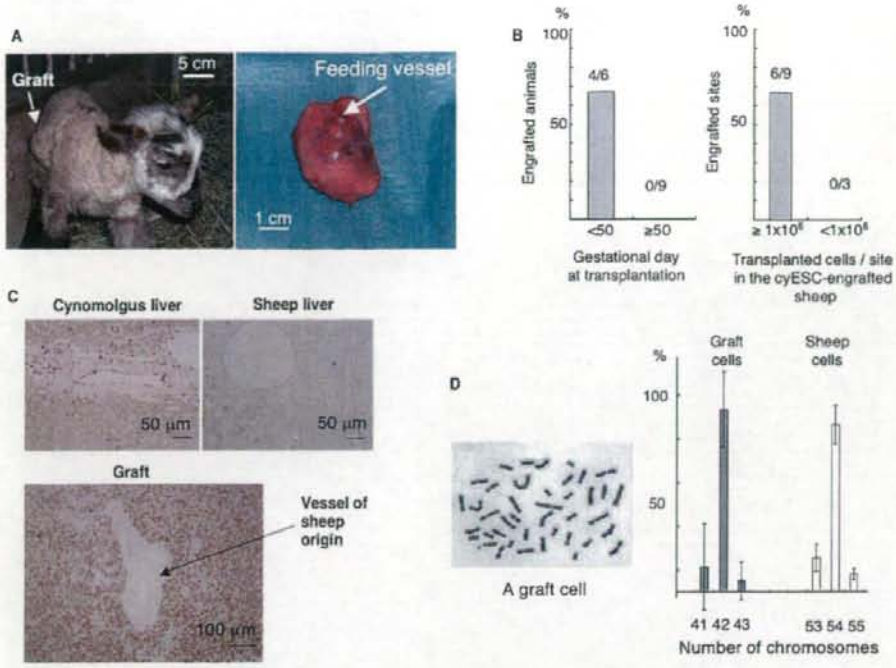

FIG. 1. Macroscopic engraftment after in utero transplantation of cyES cells into fetal sheep. (**A**) Outward appearance and macroscopic view of a tumor are shown. (**B**) The engraftment ratio (macroscopically engrafted number per total transplant number) was compared between the sheep transplanted at <50 days and ≥50 days of gestation (*left*). The engraftment ratio was also compared between $\geq 1 \times 10^6$ and $\leq 1 \times 10^6$ transplanted cells/site in the cyES cell-engrafted sheep (*right*). (**C**) In situ hybridization with the human genomic DNA probe showed that cynomolgus liver cell nuclei were stained positively, whereas sheep liver cell nuclei were not stained, indicating that the probe could be used to distinguish cynomolgus from sheep cells (*upper*). As assessed with the probe, it turned out that the tumors were of cynomolgus origin except for blood cells, some vessels, and granulated areas (*lower*). (**D**) The karyotype of tumor cells was same as that of cyES cells (*left*). The chromosome number was compared between graft and sheep cells (*right*).

cyES cells were transplanted at 48 days of gestation, GFP^+ transplanted cell progeny were detected in ductal structures 5 days later, at which time no immune cell infiltration was observed (Fig. 3A). At 2 weeks post-transplant, GFP^+ cells were found again in ductal structures (Fig. 3B), and had increased in number as suggested by the expansion of areas of GFP-derived fluorescence (Fig. 3C). A considerable number of $CD3^+$ T cells and a small number of $CD79^+$ B cells surrounded the grafts without macrophages (lysozyme-positive) (Fig. 3B). These immune cells were not stained with anti-GFP in the serial sections and thus were of host (sheep) origin. The transplanted cell progeny were still positive for Oct-3 at 2 weeks post-transplant (Fig. 3D). Staining of frozen sections showed that the surrounding T cells were $CD4^+$ and $CD8^-$ (Fig. 3E). Thus, the transplanted cells survived and proliferated, being surrounded by host $CD4^+$ $CD8^-$ T cells, when transplantation was conducted at 48 days of gestation.

When cyES cells were transplanted at 60 days of gestation, the cells were similarly detected in ductal structures 5 days later, at which time immune cell infiltration was not observed (Fig. 3F). At 2 weeks post-transplant, however, the transplantation sites were not stained with anti-GFP (Fig. 3G) and GFP-derived fluorescence was no longer detected (Fig. 3H). Instead, granulation with infiltration by T cells, B cells, and macrophages was observed (Fig. 3G). Thus, the transplanted cells were cleared away in 2 weeks when the transplantation was conducted at 60 (>50) days of gestation.

Histology II: after birth

After birth, the graft sections showed infiltration by host (sheep) T cells, fewer B cells, macrophages, and neutrophils (Fig. 4A). Most T cells were $CD4^+$, but some were $CD8^+$ (Fig. 4B). As time went on, the grafts consisted more and more of host-derived granulated tissue,